Am J Physiol Cell Physiol 315: C839–C849, 2018.
First published September 5, 2018; doi:10.1152/ajpcell.00324.2017.

RESEARCH ARTICLE

Downregulation of microRNA-149 in retinal ganglion cells suppresses apoptosis through activation of the PI3K/Akt signaling pathway in mice with glaucoma

Xin-Gang Nie, Dong-Sheng Fan, Yan-Xia Huang, Ying-Ying He, Bo-Li Dong, and Feng Gao

Department of Ophthalmology, Luoyang Central Hospital, Luoyang, People's Republic of China

Submitted 15 December 2017; accepted in final form 24 August 2018

Nie XG, Fan DS, Huang YX, He YY, Dong BL, Gao F. Downregulation of microRNA-149 in retinal ganglion cells suppresses apoptosis through activation of the PI3K/Akt signaling pathway in mice with glaucoma. *Am J Physiol Cell Physiol* 315: C839–C849, 2018. First published September 5, 2018; doi: 10.1152/ajpcell.00324.2017.—Glaucoma represents a major cause of blindness, generally associated with elevated intraocular pressure (EIOP). The aim of the present study was to investigate whether microRNA-149 (miR-149) affects retinal ganglion cells (RGCs) and the underlying mechanism based on a mouse model of chronic glaucoma with EIOP. The successfully modeled mice were administered with mimics or inhibitors of miR-149. Next, the number of RGCs, ultrastructural changes of RGCs, and purity of RGCs in the retinal tissues were detected. Moreover, the RGCs were collected and subsequently treated with 60 mmHg pressure and transfected with a series of plasmids aiding in the regulation of the expression of miR-149 and betacellulin (BTC). The levels of miR-149, BTC, phosphatidylinositol 3-kinase (PI3K), and Akt were subsequently determined. Finally, RGC viability and apoptosis were detected accordingly. Dual luciferase reporter gene assay provided validation, highlighting BTC was indeed a target gene of miR-149. The downregulation of miR-149 is accompanied by an increased number of RGCs and decreased ultrastructural RGC alterations. Additionally, downregulated miR-149 was noted to increase the levels of BTC, PI3K, and Akt in both the retinal tissues and RGCs, whereas the silencing of miR-149 was observed to promote the viability of RGC and inhibit RGC apoptosis. Taken together, the results of the current study provided validation suggesting that the downregulation of miR-149 confers protection to RGCs by means of activating the PI3K/Akt signaling pathway via upregulation of BTC in mice with glaucoma. Evidence presented indicated the promise of miR-149 inhibition as a potential therapeutic strategy for glaucoma treatment.

betacellulin; glaucoma; microRNA-149; PI3K/Akt signaling pathway; retinal ganglion cell

INTRODUCTION

As the leading cause of irreversible blindness, glaucoma is considered to be a significantly deceptive optic neuropathy, characterized by degeneration of the retinal ganglion cells (RGCs) and optic nerve damage, ultimately leading to a progressive visual field loss along with weakened contrast and color sensitivity (19). Statistical studies have presented data suggesting that 1 in 40 individuals over the age of 40 suffers from glaucoma-induced functional loss of visual field during their lifetime, suggesting that ~60 million people globally are affected, with 8.4 million people falling victim to bilateral blindness (27). Glaucoma is manifested by concomitant visual field defects at the optic nerve head and functional visual loss with elevated levels of intraocular pressure (IOP), representing the major risk factor of the condition (3, 9). Besides, there are several key factors that contribute to the etiology of glaucoma, including retinal ischemia, nutritional status, as well as oxidative stress (33). At present, the available treatment approaches for glaucoma consist of decreasing IOP, with certain antiglaucoma medications noted to be accompanied by ocular adverse reactions, including dry eyes, burning, or stinging sensations, which often fail to ameliorate the condition, leading to significant decline in the quality of life for people with glaucoma (4). RGCs function as receptor and protector of visual signals, playing crucial roles in the conveyance of visual information from the retina to visual centers in the brain (7). Therefore, it is necessary that all efforts are made in an attempt to identify novel therapeutic glaucoma strategies by elucidating the mechanism regarding the regulation of RGC proliferation and the changes of IOP, which are central factors in the treatment of glaucoma and the recovery of visual functions.

MicroRNAs (miRNAs) are a family of short endogenous noncoding RNAs, which play significant roles in the regulation of gene expressions by downregulating target genes of mRNAs or the suppression of protein translation (44). Additionally, miRNAs also function as regulators in a variety of physiological processes, including that of cell proliferation and apoptosis and consequently in the pathogenesis of numerous diseases (6). Furthermore, miRNAs have been reported to possess regulatory functions in the development and progression of glaucoma, playing critical roles in the regulation of the biological processes of glaucoma-related genes (11). A recent study indicated that progressive optic nerve neuropathy is related to altered miRNA expressions, which are observed in patients with glaucoma, suggesting that miRNAs could be responsible for neuronal cell death (23). A previous study has indicated miRNA (miR)-149 inhibits cell proliferation via the activation of the p53 signaling pathway by downregulating ZBTB2 protein in gastric cancer, leading to tumor cell arrest and hindering the growth of gastric cancer cells (36). In addition, miR-149 has been speculated to decrease potentially the rate of cell proliferation and infiltration by inhibiting the Akt1 signaling pathway in glioma cells (25). Betacellulin (BTC) is a multi-

Address for reprint requests and other correspondence: Y.-X. Huang, Department of Ophthalmology, Luoyang Central Hospital, No. 288 Zhongzhouzhong Road, Xigong District, Luoyang 471009, Henan Province, P. R. China (e-mail: huangyanxia012@yeah.net).

functional peptide growth factor that was initially understood to be a mitogen isolated from a mouse pancreatic β-cell carcinoma cell line (8). Moreover, as a member of the epidermal growth factor (EGF) family, BTC functions as a potent mitogen for certain cell types, exhibiting a higher affinity and specificity for ErbB1 and ErbB4 homodimers, influencing the activation of various signaling transduction pathways such as the phosphatidylinositol 3-kinase (PI3K)/PDK1/Akt accompanied by a series of biological effects (30). The PI3K/Akt signaling pathway by 3α-diol is involved in the regulation of cell motility and survival, as well as the formation and maintenance of optic nerve head astrocytes in glaucoma (1). Evidence has been presented indicating that PI3K could act to induce the proliferation and differentiation of the neural crest and other cellular types (31, 40). As a downstream target of PI3K, Akt kinase is closely involved in cellular processes, including the exertion of prosurvival and antiapoptotic effects, while specifically playing a critical role in the development and protection/regeneration of sensory neurons such as RGCs (16, 29). Recent studies have demonstrated that the PI3K/Akt signaling pathway plays a crucial role in modulating the activation, survival, atresia, and loss of primordial follicles in genetically modified mouse models (45), as well as suggesting the involvement of certain miRs, including miR-135a and miR-21 in non-small cell lung cancer (NSCLC; 15, 46). The PI3K/Akt signaling pathway has been demonstrated to play a role in maintaining the survival of RGCs after injury (18). Furthermore, Qi et al. (26) during their study suggested that saffron could suppress RGC apoptosis via the regulation of PI3K/Akt signaling pathway after ischemia-reperfusion. Li et al. (17) have indicated that lncRNA-MALAT1 could inhibit RGC apoptosis via the regulation of PI3K/Akt signaling pathway in rats with glaucoma. Based on the exploration of the aforementioned literature, the central objective of the present study was to investigate the mechanism of miR-149 targeting BTC on RGCs through the PI3K/Akt signaling pathway in glaucoma.

MATERIALS AND METHODS

Ethics statement. The study was conducted under the approval of the Animal Ethics Committee of Luoyang Central Hospital. All procedures were in compliance with the animal guidelines of the International Association for the Study of Pain (24).

Animal grouping. A total of 60 male and female healthy C57BL/6 mice (aged 10 ± 2 wk old and weighing 25 ± 2 g) were purchased from Guangdong Medical Laboratory Animal Center (Foshan, Guangdong, China). All recruited mice were free of any abnormalities in the outer eye and fundus oculi. Prior to the experiment, all mice were treated with 1 wk of adaptive feeding, with 3–5 mice in each cage. The mice were raised in 21°C conditions on a 12:12-h light-dark cycle, with free access to food and water and abundant space to move around. Subsequently, 60 mice were assigned randomly into five groups, as follows: *1*) normal group; *2*) elevated intraocular pressure (EIOP) group; *3*) EIOP + negative control (NC) group; *4*) EIOP + miR-149 mimic group; and *5*) EIOP + miR-149 inhibitor group (n = 12 in each group). In the event that IOP was observed to be stabilized, the fundus oculi of mice in the EIOP + NC, EIOP + miR-149 mimic, and EIOP + miR-149 inhibitor groups were, respectively, injected with NC, miR-149 mimics, and miR-149 inhibitors 10 days later (both of them were purchased from Shanghai GeneChem, Shanghai, China). Mice in the normal group were administered by identical doses of normal saline once a day for 15 days.

Establishment of mouse models of chronic glaucoma with EIOP. The mouse glaucoma model with chronic EIOP was established by means of episcleral venous occlusion with cauterization. Prior to establishment, the C57BL/6 mice were intraperitoneally injected with 1% pentobarbital sodium (cat. no. P-3761, 50 mg/kg, Sigma Aldrich, St. Louis, MO) for general anesthesia means, with their ocular surfaces anesthetized twice dropwise with pentobarbital sodium. The bulbar conjunctiva at the limbus was severed at the superior temporal, the inferior temporal, and the superior nasal quadrants. After the extraocular muscles and fascia were separated, three proximal episcleral veins were found and cauterized with a disinfected pin allowing for congestion of the proximal and distal veins, which turned white (32). The left eye of the mice served as the untreated controls. Before and after model establishment, the conjunctival sac was washed with the mixture of gentamicin injection (cat. no. G-3632; Sigma Aldrich) and saline. After model establishment, the ocular region was treated with erythromycin ophthalmic ointment (HYA006016D; Chen Xin Pharmaceutical, Beijing, China) to alleviate the levels of inflammation three times a day for 3 days. Ten days later, the model was considered to have been successfully established in the event that the average IOP was observed to be maintained above 22 mmHg (1 mmHg = 0.133 kPa).

Measurement of EIOP. A Tono-Pen AVIA handheld tonometer (Reichert Ophthalmic Instrument, Depew, NY) was employed to measure the IOP of mice in the normal group and the EIOP group before (0 days) and after model establishment (3, 10, 20, and 30 days), whereas the incidence of inflammation in the cornea and conjunctiva was recorded. Before IOP measurement, surface anesthetic drops were administered twice to the eyes of the mice. IOP was measured by the same person at 1500 to avoid manual errors and provide an additional degree of control in the experiment. The eye of each mouse was measured twice each time, with evaluation conducted using a trusted domain and if found to be below 90% was discarded. The mice eyes were washed with diluted gentamicin after measurement. A total of 12 mice in each group were all measured as the above-mentioned procedures, and then the measured data were recorded.

Hematoxylin-eosin staining. The mice in all groups were euthanized after 15 days of administration. The eyeballs of mice were then removed and fixed in 4% paraformaldehyde (cat. no. P-1110; Beijing Solarbio Science & Technology, Beijing, China). The cornea was cut along the sclera, with the iris and crystalline lens removed 30 min later. The retina was cryprotected overnight in 30% sucrose and then embedded in optimal cutting temperature. Subsequently, the retina was sliced into serial sections with a thickness of 5 μm and stored at −20°C for further use. The frozen tissues were stained with hematoxylin (cat. no. G-1140, Beijing Solarbio Science & Technology) for 7 min and washed with running water for 1 min, followed by immersion in 1% hydrochloric acid-ethanol for 15 s and an additional 4 min of washing with running water. Afterwards, the sections were stained with eosin for 3 min, followed by dehydrating in 70%, 80%, and 90% gradient ethanol for 1 min in a successive manner, followed by dehydration with 95% ethanol for 2 min, as well as in 100% ethanol I and ethanol II for 5 min, respectively. The sections were cleared in xylene I and xylene II for 10 min each and sealed with neutral gum. Finally, the sections were observed under an optical microscope (×200) (BX-51, Olympus, Tokyo, Japan) with a red cytoplasm and blue nucleus, and then five visual fields of each sample were randomly selected to count the RGCs. Next, the SE IPS image analyzer was employed to measure the thickness of the ganglion cell layer (GCL) and inner plexiform layer (IPL) of the sections which were stained by hematoxylin-eosin. Three sections from five mice in each group were selected and determined.

Electronic microscopic observation. The retinal tissues of the inferior temporal lobe were extracted and embedded with Durcupan (cat. no. 44612; Sigma Aldrich) and sliced into 0.5-μm sections. After staining with uranyl acetate and lead citrate, the morphology of the RGCs in the sections were observed and photographed under a

H-7500 transmission electron microscope (×15,000) (Hitachi, Tokyo, Japan). Three sections from three mice in each group were taken and three visual fields were randomly selected in each tissue section.

TUNEL staining. The frozen retina sections were taken out and then placed into a wet box after they were brought back to room temperature. The sections were immersed in formaldehyde with 3% H_2O_2 for 30 min to block endogenous peroxidase activity, followed by phosphate-buffered saline (PBS) washing. Permeabilizing reagent was added to the cells and permitted to react for 20 min, followed by PBS washing. TUNEL mixture was added to the cells and incubated under conditions void of light at 37°C for 20 min, followed by PBS washing. The sections were subsequently added with 50 μl of POD transforming agent (11684817910; Roche, Mannheim, Germany) for incubation under conditions void of light at 37°C for 1 h. The sections were developed by diaminobenzidine tetrahydrochloride (DAB) (ZLI-9032; Beijing Zhongshan Jinqiao Biotechnology, Beijing, China), counter-stained by hematoxylin, rinsed with running water, dried, and mounted. Five visual fields in each section were selected randomly and observed under a light microscope (×200). The cells presenting with yellow particles in the nuclei or cytoplasm were considered to be the positive cells. ImageJ software (NIH, Bethesda, MD) was used for image analysis and counting. Five fields under the high-power microscope (10 × 40) and 200 cells were randomly selected to calculate the positive cells. The percentage of positive cells was considered to be representative of the cell apoptosis percentage. Retinal tissues from five mice in each group were cut into three sections on a freezing microtome. Then three visual fields were selected in each tissue section.

RGC isolation and culture. A total of 10 C57BL/6 mice (aged 4–6 days) were decapitated under sterile conditions, with the retina isolated under an anatomical microscope. The isolated retina was then digested with 0.125% trypsin and placed at 37°C for 20 min. The digested retina was subsequently centrifuged at a rate of 179 *g* to discard the supernatant. After being neutralized with 0.25% trypsin inhibitor (cat. no. T-9003; Sigma Aldrich), the retina was centrifuged to discard the supernatant. The retina was rinsed three times with Kreb solutions composed of magnesium and 1% bovine serum albumin (BSA). Following the addition of the culture medium, the cells were triturated and dispersed by a tubularis. The single-cell suspension at a density of 1×10^6 cells was placed in the culture dish covered by 0.1 mg/ml of poly-L-ornithine (cat. no. P-4538; Sigma Aldrich) and 1 μg/ml of laminin (cat. no. l-6274, Sigma Aldrich). Finally, Basal Medium Eagle (BME) culture medium (cat. no. SBJ-ME1268; Nanjing SenBeiJia Biological Technology, Nanjing, Jiangsu, China) containing 10% fetal bovine serum, 25 μmol/l glutamine, and 0.1 mg/ml gentamicin was added to the cells and incubated in a 5% CO_2 incubator at 37°C with saturated humidity (12, 37, 42).

Purification and identification of RGCs. The retina single-cell suspension was placed in the BME culture medium consisted of goat anti-mouse IgG antibody (cat. no. ab-6785; 1:1,000; Abcam, Cambridge, MA) and rat anti-mouse Thy-1.1 antibody (cat. no. ab-44898; 1:1,000; Abcam) and incubated at 37°C for 30 min to ensure the RGCs adequately combined with Thy-1.1 antibody. Cell suspension was then discarded and the cells were rinsed three times with BME. After discarding the nonadherent cells, the RGCs were incubated with 0.125% trypsin for 10 min, with the adherent RGCs collected, followed by counting and culturing. The purified RGCs were cultured for 4 h before culture medium removal and fixed in 4% paraformaldehyde for 4 h. After 3 PBS washes, the RGCs were added with monoclonal antibody of rat anti-mouse FITC-Thy1.1, followed by 30-min incubation at 37°C and an additional 3 PBS washes. Finally, 12 visual fields were randomly selected, observed, and photographed under a fluorescence microscope (BX-51; Olympus, Japan, Tokyo, Japan) as well as a phase contrast microscope. In the same visual field, the purity of RGCs was the ratio of positive cells observed using a fluorescence microscope, whereas the total cells were observed using phase contrast microscope (12, 37, 42). RGC identification was repeated three times.

Cell grouping and transfection. The RGCs were subsequently assigned into seven groups, namely: the control group (RGCs were cultured without pressure), the pressure group (60 mmHg, RGCs were cultured with pressure), the pressure + NC group (60 mmHg, RGCs were cultured with compression and NC), the pressure + miR-149 mimic group (60 mmHg, RGCs were cultured with compression and miR-149 mimic), the pressure + miR-149 inhibitor group (60 mmHg, RGCs were cultured with compression and miR-149 inhibitor), the pressure + siBTC group (60 mmHg, RGCs were cultured with compression and siBTC) and the pressure + miR-149 inhibitor + siBTC group (60 mmHg, RGCs were cultured with compression, miR-149 inhibitor siBTC) (21). One day before transfection, cells at a density of 1×10^5 were seeded into a 24-well plate, with 500 μl of antibiotic-free medium added to each well. When cell confluence reached 50%–70%, the RGCs were transfected in a respective manner with miR-149 inhibitors, miR-149 mimics, and siBTC plasmids according to the Lipofectamine 2000 Reagent. The plasmid was synthesized by Shanghai Genechem (Shanghai, China). Besides, the plasmid/liposome complexes were compounded in sterile Eppendorf tube: 12 μl of lipofectamine 2000 and 500 μl of serum-free medium, which was then permitted to stand at room temperature for 5 min and 6 mg of empty plasmid and 500 μl of serum-free medium, permitted to stand at room temperature for 20 min allowing the DNA and liposome complexes to form; cells were then washed with serum-free medium. Serum-free and antibiotic-free medium was then added to the complexes and shaken gently, followed by transferal to the pretransfected cell culture dishes. The cells were then incubated at 37°C with 5% CO_2. After 6–8 h, the culture medium was replaced with a complete culture medium, and the cells were incubated by adding pressure for 2 h. The pressure was set as 60 mmHg (according to the fluctuation range of IOP in glaucoma disease, the pressure was added to 60 mmHg with O_2 containing 5% CO_2 in closed cabinet, which met the basic operation principles of CO_2 cell incubator with stable CO_2 of 5%, constant pH value of 7.2–7.4, constant temperature of 36°C–37°C, and relatively higher humidity of 95%. The pressure regulating range was 1–100 mmHg). The samples were subsequently incubated for a further 24–48 h. Three repeated holes were set in each experiment. After that, the cells were then collected for the following experiments. The aforementioned cell grouping and transfection were repeated three times.

Table 1. *Primer sequences for RT-qPCR*

Gene	Primer Sequence (5′–3′)
miR-149	
Forward	TGGCTCCGTGTCTTCACTCCC
Reverse	CAGTGCAGGGTCCGAGGTAT
U6	
Forward	CGCTTCGGCAGCACATATAC
Reverse	TTCACGAATTTGCGTGTCAT
BTC	
Forward	CTCCAAATGGAACTATGGAA
Reverse	CATGATATTAAGCAGCTGTG
PI3K	
Forward	TGTGGCACAGACTTGGTGTT
Reverse	TTCTTCCCTTGAGATGTCTCCC
Akt	
Forward	CCGCCTGATCAAGTTCTCCT
Reverse	TTCAGATGATCCATGCGGGG
β-Actin	
Forward	GTCGAGTCGCGTCCACC
Reverse	CTCATCCATGGCGAACTGGT

BTC, betacellulin; miR-149, microRNA-149; PI3K, phosphatidylinositol-3-kinase; RT-qPCR, reverse transcription quantitative polymerase chain reaction.

Table 2. *Changes in IOP after surgery in normal and EIOP groups*

Group	Time Point				
	0 days	3 days	10 days	20 days	30 days
EIOP group, mmHg	15.62 (2.24)	24.27 (2.52)*	31.52 (3.21)*	33.61 (2.74)*	32.74 (3.04)*
Normal group, mmHg	16.26 (2.42)	17.26 (2.14)	16.43 (2.56)	16.88 (2.18)	17.05 (2.23)

Values are means (SD); $n = 12$. EIOP, elevated intraocular pressure; IOP, intraocular pressure. *$P < 0.05$ vs. normal group (Student's *t*-test; experiment repeated 3 times).

Dual luciferase reporter gene assay. RNA22 (https://cm.jefferson.edu/rna22/) was employed to help predict the target genes of miR-149. The sequence containing the binding site of miR-149 in the 3′-untranslated region (3′UTR) of BTC was constructed artificially, to obtain the target sequence of BTC-wild-type (Wt) 3′UTR and target sequence of BTC-mutant (Mut) 3′UTR. The target fragments were then inserted into the vector of pGL3-Lucifearse (Promega, Madison, WI) through enzyme digestion of Xho I and Not I to obtain the Wt and Mut plasmids. Following the verification of the sequences, the above plasmids were cotransfected with miR-149 mimic and NC into 293T cells, respectively. After 48 h of transfection, the cells were collected and treated with cell lysate. A dual luciferase reporter gene assay kit (Dual-Luciferase Reporter Assay System; cat. no. E-1910; Promega Corp., Madison, WI) was applied for the examination of luciferase activity. Each cell sample was added with 100 μl of the working fluid of firefly luciferase to detect the activity of firefly luciferase, and 100 μl of the working fluid of renilla luciferase was used to help detect the activity of renilla luciferase. Finally, the relative luciferase activity was calculated. There repeated holes were set and the above mentioned target gene prediction, plasmid transfection, and luciferase activity examination were repeated three times independently.

RNA extraction and reverse transcription quantitative polymerase chain reaction. Total RNA was extracted from the tissues and cells from all groups using the Trizol reagent (cat. no. 15596026; Invitrogen, Carlsbad, CA). Ultraviolet spectroscopy was applied to detect the value of OD260/280 of each RNA sample, followed by determination of the RNA concentration. The RNA samples were stored at −80°C for further use. Reverse transcription of RNA was performed in accordance with the instructions of the Reverse Transcription Reagent kit (cat. no. K-1622, Fermentas, Hanover, MD), followed by dilution of the product five times by sterile water and stored at −20°C. The primer sequences of miR-149, BTC, PI3K, and Akt were synthesized by Shanghai Genechem (Shanghai, China) illustrated in Table 1. Reverse transcription quantitative polymerase chain reaction (RT-qPCR) was performed with the reaction system with a total volume of 23.5 μl, including 12.5 μl of SYBR Premix EX TaqTM, 1 μl of cDNA, 0.5 μl of forward primers (10 μM), and 0.5 μl of reverse primers (10 μM) and 9.5 μl of sterile water. The reaction conditions consisted of predegeneration at 94°C for 3 min, followed by 30 cycles of degeneration at 94°C for 30 s, annealing at 58°C for 30 s, and extension at 72°C for 60 s. RT-qPCR was conducted using the ABI 7500 PCR instrument (ABI, Foster City, CA). There were three preset wells for each

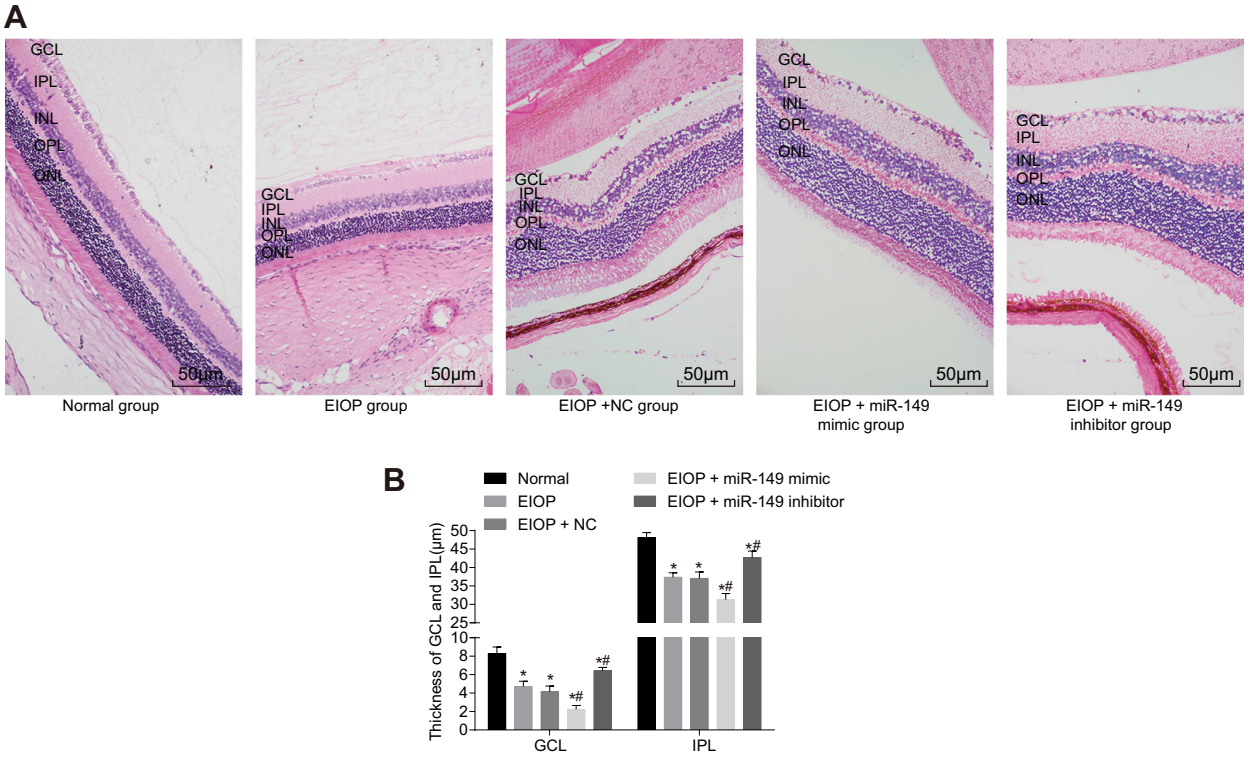

Fig. 1. HE staining reflects that downregulation of miR-194 attenuates glaucoma (×200). *A*: images of frozen retinal sections under a light microscope using HE staining. Scale bar = 50 μm. *B*: thickness of GCL and IPL; *$P < 0.05$ vs. the normal group; #$P < 0.05$ vs. the EIOP and EIOP + NC groups. $n = 5$; measurement data are expressed as means ± SD; one-way analysis of variance was used to analyze data. EIOP, elevated intraocular pressure; GCL, ganglion cell layer; HE, hematoxylin and eosin; IPL, inner plexiform layer; INL, inner nuclear layer; OPL, outer plexiform layer; ONL, outer nuclear layer; miR-149, microRNA-149; NC, negative control.

Table 3. *Number of RGCs after 15 days of administration*

Group	No. of Cells/480 μm
Normal	26.67 (2.27)
EIOP	15.00 (2.04)*
EIOP + NC	16.08 (2.35)*
EIOP + miR-149 mimic	8.83 (1.27)*†
EIOP + miR-149 inhibitor	21.92 (2.61)*†

Values are means (SD); $n = 5$. EIOP, elevated intraocular pressure; miR-149, microRNA-149; NC, negative control; RGCs, retinal ganglion cells. *$P < 0.05$ vs. normal group; †$P < 0.05$ vs. EIOP group and EIOP + NC group (one-way ANOVA; experiment repeated 3 times).

gene. U6 was regarded to be the miR-146 internal reference, whereas β-actin served as the internal reference of BTC, PI3K, and Akt. A melting curve was constructed to assess the viability of the RT-qPCR results. The $2^{-\Delta\Delta Ct}$ method was applied for the measurement of relative expression of the target gene. $\Delta\Delta Ct = \Delta Ct_{\text{experimental group}} - \Delta Ct_{\text{control group}}$ and $\Delta Ct = Ct_{\text{target gene}} - Ct_{\beta\text{-actin}}$. The RNA extraction and detection of RGCs and proteins of retina tissues in each group repeated three times as aforementioned.

Western blot analysis. Total protein of the cells and tissues was extracted, with the protein concentration measured based on the instructions of the BCA kit (cat. no. 23227, Pierce, Rockford, IL). Protein was separated by 10%, with the separation voltage altered from 80 V to 120 V. Protein was then transferred to the PVDF membrane via a wet transfer method for 45–70 min with the transfer voltage of 100 mV and blocked with 5% BSA for 1 h. According to the size of each target band, the bands corresponding to the target protein were taken, respectively, which separately corresponded to the following primary antibodies: rabbit anti-mouse primary antibody BTC (1:1,000; cat. no. ab-185702; Abcam), PI3K (1:1,000; cat. no. ab-40776; Abcam), p-PI3K (1:1,000, cat. no. ab-182651; Abcam), Akt (1: 500, cat. no. ab-8805; Abcam), p-Akt (1: 500, cat. no. ab-38449; Abcam), and GAPDH (1:2,500, cat. no. ab-9485; Abcam). In the next step, these antibodies were added in a successive manner into the membrane for incubation for 30 min and placed in a freezer at 4°C overnight. The membrane was then washed three times with Tris-buffered saline Tween 20 (10 min per time). Next, the corresponding second antibodies were added to the samples for incubation at room temperature for 2 h, followed by washing of the membranes. The protein membrane was then treated with a color-developing agent. Protein photographs were developed and fixed after box exposure. The images were analyzed by the ImageJ analysis software. GAPDH served as the internal reference. The extraction procedures of RGCs and proteins of retina tissues in each group were processed three times as aforementioned.

Cell counting kit-8 assay. After pressure added incubation for 24 h, the RGCs were collected and treated with 0.25% trypsin to construct a single-cell suspension with a cell density of 5×10^5 cells/ml. The cell suspension (0.1 ml per well) was then added to the 96-well plate, with each group preset with 6 repeat wells. Next, 10 μl of cell counting kit-8 solution (cat. no. CK-04, Dojindo, Kumamoto, Japan) was added to each well for color development and incubated in a 37°C incubator with 5% CO_2 for 4 h. After culture medium removal, the optical density value was measured using an automatic microplate reader at 450 nm (iMark, Bio-Rad, Hercules, CA), and cell viability was calculated. Cell viability determination was conducted three times independently as described previously.

Annexin V-fluoroscein isothiocyanate-propidium iodide assay. After pressure-added incubation for 24 h, RGCs were collected and digested with EDTA-free trypsin after 24 h. The mixture was then centrifuged at a rate of 716 *g* at room temperature for 5 min, followed by collection of the cells. The cells were resuspended with 1 ml of cold PBS and then centrifuged at a rate of 716 *g* for 5 min. After supernatant removal, the cells were resuspended in 300 μl of binding buffer. Next, 5 μl of annexin V-FITC (cat. no. CA-1020; Beijing Solarbio Science & Technology) was added to the cells, and then cells were permitted to stand at room temperature for 15 min under conditions void of light. A total of 5 μl of propidium iodide was added to the cells for 5-min staining. After the addition of 200 μl Binding Buffer, cell apoptosis was detected by flow cytometry (FACSCalibur, Becton Dickinson, Sunnyvale, CA) with the rate of apoptosis calculated in each group. The formula applied was as follows: apoptotic rate = (apoptotic cells in the early phase + apoptotic cells in late phase)/the total number of cells × 100%. Cell apoptosis measurement was performed three times as the above mentioned.

Statistical analysis. Statistical analysis was performed using the SPSS 21.0 software (IBM Corp. Armonk, NY). Measurement data was presented as means ± SD. Comparisons between two groups were conducted by Student's *t*-test. Comparisons among multiple groups were assessed using one-way analysis of variance (ANOVA, and evaluated by Bonferroni's multiple comparison test. $P < 0.05$ was considered to be indicative of statistical significance.

RESULTS

Successful establishment of EIOP mouse models. The IOP of mice was measured before and after model establishment. Prior to model establishment (0 days) with EIOP, the mean IOP was 15.62 mmHg (SD 2.24). After surgical treatment, the mean IOP exhibited varying figures at different time points, which was as follows: 24.27 mmHg (SD 2.52) (3 days); 31.52 mmHg (SD 3.21) (10 days), 33.41 mmHg (SD 2.74) (20 days), 32.58 mmHg (SD 3.04) (30 days). The mean IOP was significantly different from those in normal group at different time points after surgery (all $P < 0.05$, Table 2). Ten days later, after successful mouse model establishment, the IOP was stable and mice were treated with drug injection for the following experiments.

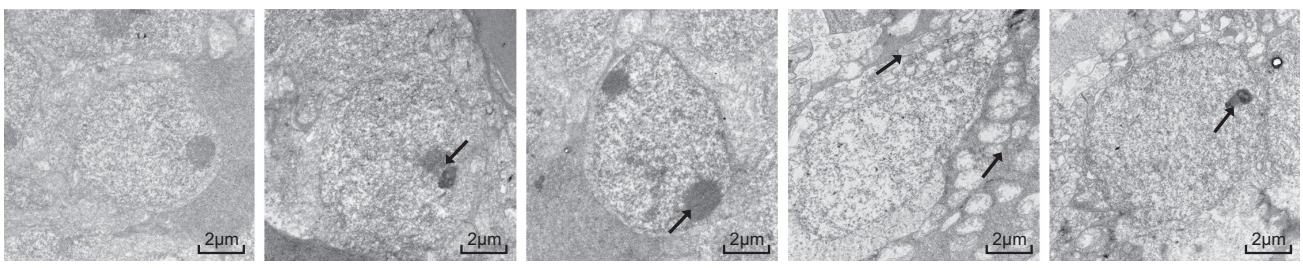

Fig. 2. Downregulation of miR-149 reduces ultrastructural changes of RGCs (×15,000). Scale bar = 2 μm. Arrows refer to demarcation membrane between nucleus and cytoplasm and porphyry and vacuoles in substrate resulting from hydration-induced metamorphism. EIOP, elevated intraocular pressure; miR-149, microRNA-149; NC, negative control; RGCs, retinal ganglion cells; $n = 3$.

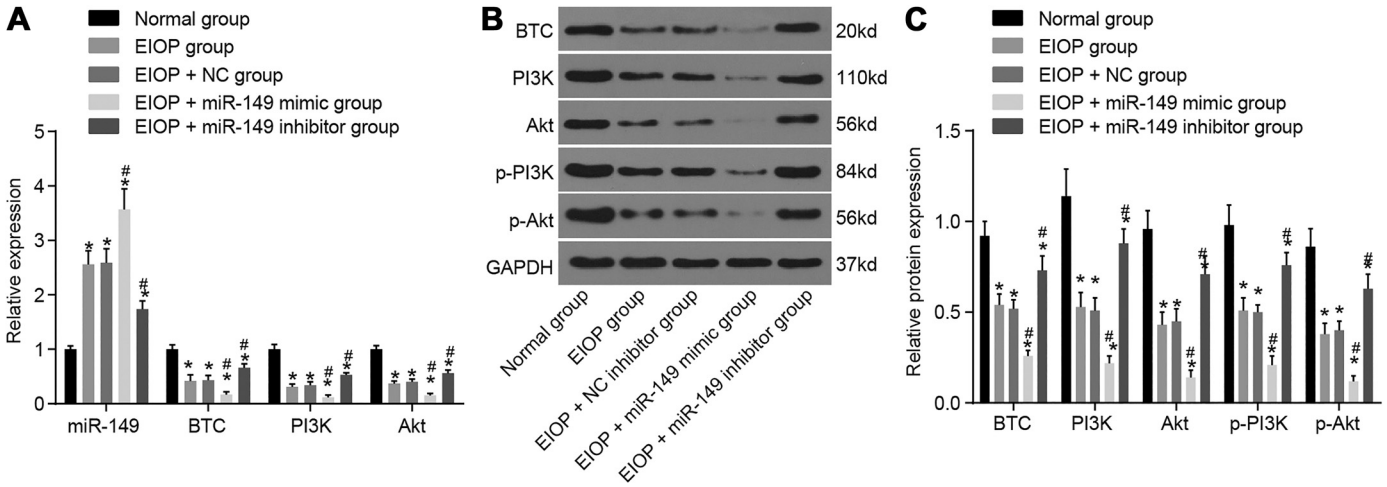

Fig. 3. RT-qPCR and Western blot analysis show that downregulation of miR-149 increases expression levels of BTC, PI3K, and Akt in retinal tissues. *A*: RT-qPCR was used to determine expression levels of miR-149 and mRNA expression of BTC, PI3K, and Akt in retinal tissues. *B*: protein bands patterns of BTC, PI3K, p-PI3K, Akt, and p-Akt using Western blot analysis. *C*: protein levels of BTC, PI3K, p-PI3K, Akt, and p-Akt using Western blot analysis. $*P < 0.05$ vs. normal group; $\#P < 0.05$ vs. EIOP and EIOP + NC groups; $n = 4$. Measurement data are expressed as means ± SD; one-way analysis of variance was used to analyze data; the experiment was repeated 3 times. BTC, betacellulin; EIOP, elevated intraocular pressure; miR-149, microRNA-149; NC, negative control; PI3K, phosphatidylinositol-3-kinase; RGCs, retinal ganglion cells; RT-qPCR, reverse transcription quantitative polymerase chain reaction.

Downregulation of miR-194 attenuates glaucoma and increases the number of RGCs in EIOP models. Hematoxylin-eosin staining was used to analyze the pathological changes of the retina. The tissues were examined 15 days after administration, as shown in Fig. 1. Compared with normal mice, the IPL in the ocular hypertension groups were thinned to different extents and the cells in GCL were fewer to varying degrees. The IPL was thinner and the cells in GCL much fewer in the ocular hypertension + miR-149 mimic group than that in the ocular hypertension group and the high intraocular pressure + NC group. However, IPL was significantly thicker and GCL cells were significantly increased in the high intraocular pressure + miR-149 inhibitor group when compared with the ocular hypertension group and the high intraocular pressure + NC group.

After injection for 15 days, the mice retinal tissues morphological changes were observed (Table 3); the number of RGCs in the EIOP groups was lower than that in the normal group (all $P < 0.05$). Besides, decreased amount of RGCs was detected in the EIOP + miR-149 mimic group when comparison to the EIOP and EIOP + NC groups (both $P < 0.05$), whereas the EIOP + miR-149 inhibitor group exhibited a significantly increased number of RGCs in comparison to the EIOP and EIOP + NC groups (both $P < 0.05$). These findings suggested that silencing miR-194 may likely result in an increase in the number of RGCs in the EIOP models.

Downregulation of miR-149 reduces ultrastructural changes of RGCs. After 15 days of treatment had elapsed, the ultrastructural changes of RGCs in retinal tissues of mice were detected accordingly, the results of which are illustrated in Fig. 2. The RGCs in the normal group were observed to be oval-shaped, with normal morphology and perinuclear space as well as even chromatin distribution. The RGCs were characterized by unclear margination phenomenon, complete cytoplasm membrane with no signs of edema within the organelle. Meanwhile, in the EIOP, EIOP + NC and EIOP + miR-149 mimic groups, we observed RGCs with nuclear membrane invagination, karyopyknosis, irregular morphology, widened perinuclear space, uneven chromatin distribution, as well as the distinct phenomenon of margination. In the EIOP + miR-149 mimic group, RGCs displayed an incomplete cytoplasm membrane, broken borders, advanced edema, as well as hydration in mitochondria, endoplasmic reticulum, and the Golgi apparatus as well in other organelles, with porphyritic, vacuolated, and even bullous electron lucent regions. Moreover, in the EIOP + miR-149 inhibitor group, RGCs were observed to have an oval-shaped nucleus, regular morphology, widened perinuclear space, even chromatin distribution, unclear margination phenomenon, complete cytoplasm membrane, as well as no signs of edema within the organelles. The above results provided convincing evidence that downregulation of miR-149 could reduce the ultrastructural changes of the RGCs.

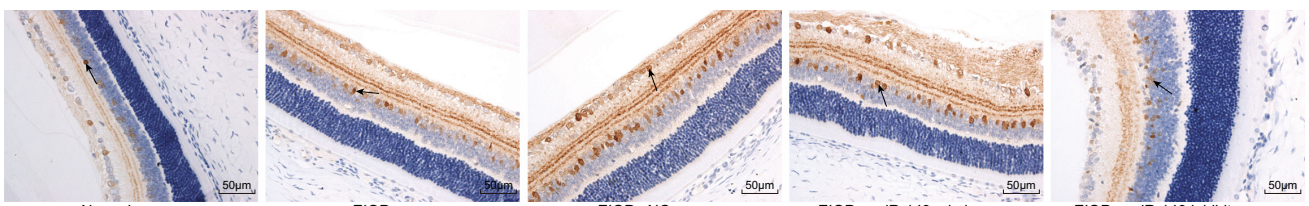

Fig. 4. TUNEL shows that downregulation of miR-149 inhibits apoptosis of positive RGCs in EIOP (×200). Arrow refers to apoptotic positive RGCs. Scale bar = 25 μm; $n = 4$. EIOP, elevated intraocular pressure; RGCs, retinal ganglion cells; miR-149, microRNA-149; NC, negative control; TUNEL, terminal deoxynucleotidyl transferase-mediated dUTP-biotin nick end labeling.

Table 4. *Positive rate (%) of apoptotic RGCs in retina of C57BL/6 mice among groups (%)*

Group	Rate, %
Normal	1.05 (0.36)
EIOP	44.07 (5.52)*
EIOP + NC	45.62 (4.85)*
EIOP + miR-149 mimic	57.72 (6.13)*†
EIOP + miR-149 inhibitor	22.47 (3.22)*†

Values are means (SD); $n = 5$. EIOP, elevated intraocular pressure; miR-149, microRNA-149; NC, negative control; RGCs, retinal ganglion cells. *$P < 0.05$ vs. normal group; †$P < 0.05$ vs. EIOP group and EIOP + NC group (one-way analysis of variance).

Downregulation of miR-149 increases the expression levels of BTC, PI3K, and Akt in the retinal tissues. After 15 days of treatment had elapsed, RT-qPCR and Western blot analysis methods were performed to determine the expression level of miR-149, as well as mRNA and protein levels of BTC, PI3K, and Akt in retinal tissues. Compared with the normal group, the EIOP groups showed significantly elevated levels of miR-149 expression as well as obvious reductions of mRNA and protein levels of BTC, PI3K, and Akt (all $P < 0.05$). There was no significant difference observed between the EIOP group and the EIOP + NC group in the miR-149 expression level, as well as mRNA and protein levels of BTC, PI3K, and Akt (all $P > 0.05$). In comparison to the EIOP and EIOP + NC groups, the EIOP + miR-149 mimic group displayed significantly ascended expression levels of miR-149, although significantly decreased mRNA and protein levels of BTC, PI3K, and Akt. Moreover, in the EIOP + miR-149 inhibitor group, the miR-149 expression levels were significantly decreased, whereas the mRNA and protein levels of BTC, PI3K, and Akt exhibited notable increases (all $P < 0.05$) (Fig. 3). The aforementioned results suggest a potential important role of miR-149 downregulation in increasing the expression levels of BTC and promoting the activation of the PI3K/Akt signaling pathway in retinal tissues.

Downregulation of miR-149 inhibits apoptosis of positive RGCs in EIOP. After 15 days of continuous injections, the mice retinal tissues were collected for RGC apoptosis detection by means of TUNEL analysis. The apoptotic-positive RGCs were represented by a brown-yellow cell cytoplasm or nucleus, whereas the negative RGCs were represented by blue. Furthermore, the majority of positive RGCs were determined to be located in the GCL of the retina. Compared with the normal group, all EIOP groups exhibited significantly substantial increases in the positive rate of the apoptosis of RGCs (all $P < 0.05$). There was no significant difference observed between the EIOP group and the EIOP + NC group ($P > 0.05$). Compared with the EIOP and EIOP + NC groups, the EIOP + miR-149 mimic group displayed a distinct increase in the rate of apoptosis of the positive RGCs, whereas the EIOP + miR-149 inhibitor group exhibited a contrasting trend (all $P < 0.05$) (Fig. 4, Table 4). The above findings revealed that silencing miR-149 may likely suppress apoptosis of positive RGCs in EIOP.

Identification of RGCs. Immunofluorescence staining was applied to identify the purity of RGCs. The RGCs were identified in connection with immunofluorescent monoclonal antibody staining with the specific marker FITC-Thy-1.1. The RGCs were visualized under a fluorescence microscope with the positive elements signified by yellow-green fluorescence on the surface of the cell membrane and sections of the cell protuberance. Ten visual fields were selected at random to calculate the purity of RGCs, the result of which was confirmed to be 95.72% (Fig. 5).

miR-149 negatively targets BTC. There is evidence (https://cm.jefferson.edu/rna22/) suggesting that BTC was the target gene of miR-149, which was then further verified in connection with a luciferase report. Based on the predication of the online software, the determined binding sites of miR-149 and BTC 3′UTR are depicted in Fig. 6*A*. BTC was found to be a target gene of miR-149. According to Fig. 6*B*, the luciferase activity was significantly reduced in BTC-WT of the miR-149 mimic group ($P < 0.05$). However, there was no significant difference in relation to the luciferase activity of Mut plasmid, when compared with that of the NC group ($P > 0.05$). These results suggested that miR-149 could bind with BTC and downregulate BTC expression.

Downregulation of miR-149 increases expression levels of BTC, PI3K, and Akt in RGCs. In the cell experiment, RT-qPCR and Western blot analysis methods were applied to determine the expression levels of miR-149, as well as the mRNA and protein levels of BTC, PI3K, and Akt in RGCs. When compared with the control group, miR-149 expression level increased, whereas expression levels of BTC, PI3K, and Akt decreased in the other pressure groups (all $P < 0.05$). There was no significant difference detected between the pressure and pressure + NC groups (all $P > 0.05$). Compared with the pressure and pressure + NC groups, the pressure + miR-149 mimic group displayed an increased expression level of miR-149 and decreased expression level of BTC, PI3K, and Akt (all

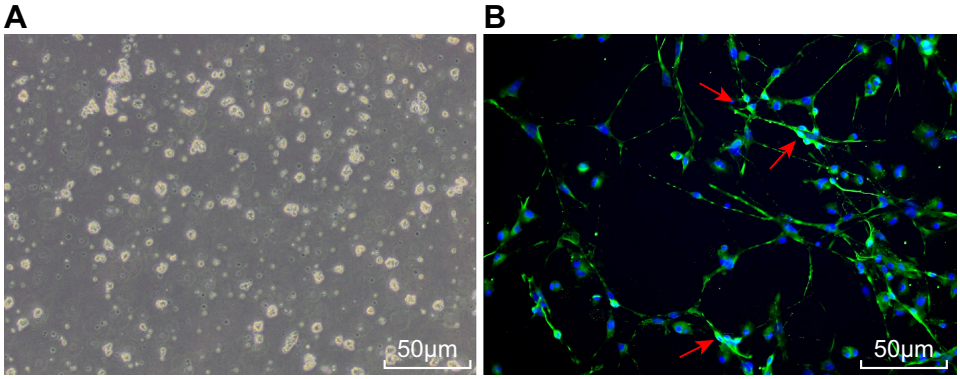

Fig. 5. Immunofluorescence staining reflects the purity of RGCs. *A*: morphological observation of RGCs (×200). Scale bar = 50 μm. *B*: immunofluorescence of RGCs (×200). Scale bar = 50 μm. Arrow refers to positive RGCs. The experiment was repeated 3 times. miR-149, microRNA-149; RGCs, retinal ganglion cells.

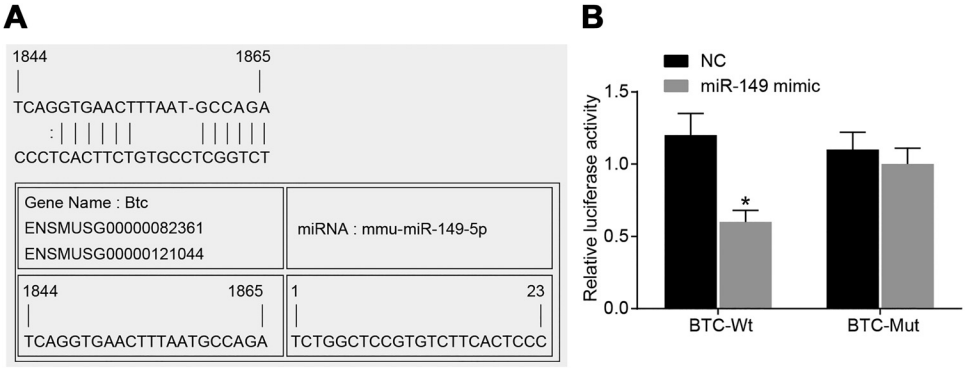

Fig. 6. Dual-luciferase reporter gene assay shows that miR-149 negatively targets BTC. *A*: sequence in the 3′-UTR of binding sites of miR-149 and BTC. *B*: detection of luciferase activity by dual luciferase reporter gene assay; BTC-Wt refers to wild-type plasmids in the 3′-UTR containing BTC; BTC-Mut refers to the mutant plasmids in the 3′-UTR containing BTC. $*P < 0.05$ vs. NC group; $n = 5$; the experiment was repeated 3 times. BTC, betacellulin; Mut, mutant; UTR, untranslated region; miR-149, microRNA-149; NC, negative control; RGCs, retinal ganglion cells; Wt, wild type.

$P < 0.05$), whereas the pressure + miR-149 inhibitor and pressure + siBTC groups exhibited a contrasting trend (all $P < 0.05$), with no significant difference observed in the pressure + miR-149 inhibitor + siBTC group in terms of the expression levels of BTC, PI3K, and Akt (all $P > 0.05$) (Fig. 7). Considering these findings, we reasoned that silencing miR-149 can increase expression levels of BTC and promote activation of the PI3K/Akt signaling pathway in RGCs.

Downregulation of miR-149 promotes RGC viability. CCK-8 assay was employed to determine the RGC viability. As shown in Fig. 8, when compared with the control group, decreased cell viability was discovered in the other groups (all $P < 0.05$). There was no significant difference detected in relation to cell viability between the pressure and pressure + NC groups ($P > 0.05$). In comparison to pressure and pressure + NC groups, the pressure + miR-149 mimic group and the pressure + siBTC group exhibited a decline in cell viability, whereas the pressure + miR-149 inhibitor group presented an opposite trend (all $P < 0.05$). No significant difference was detected in the pressure + miR-149 inhibitor + siBTC group in relation to cell viability as compared with the pressure and pressure + NC groups (both $P > 0.05$). These results revealed that silencing miR-149 could promote RGC viability.

Downregulation of miR-149 inhibits RGC apoptosis. Flow cytometry was employed to detect RGC apoptosis. Compared with the control group, RGC apoptotic rate in other groups was significantly increased (all $P < 0.05$). No significant difference was observed in terms of cell apoptosis between the pressure and pressure + NC groups ($P > 0.05$). Compared with the pressure and pressure + NC groups, the rate of apoptosis was markedly increased in the pressure + miR-149 mimic and pressure + siBTC groups but decreased in the pressure + miR-149 inhibitor group (all $P < 0.05$), with cell apoptosis in the pressure + miR-149 inhibitor + siBTC group exhibiting no distinct difference ($P > 0.05$) (Fig. 9). The obtained results revealed that silencing of miR-149 could inhibit RGC apoptosis.

DISCUSSION

Implicated in the occurrence and progression of multiple cancers, miR-149 is functionally considered to be a regulator in the processes of proliferation and apoptosis, with reports suggesting it to be a potential therapeutic target for the treatment of various types of cancers (20, 39). A previous study investigating the PI3K/Akt signaling pathway highlighted its in-

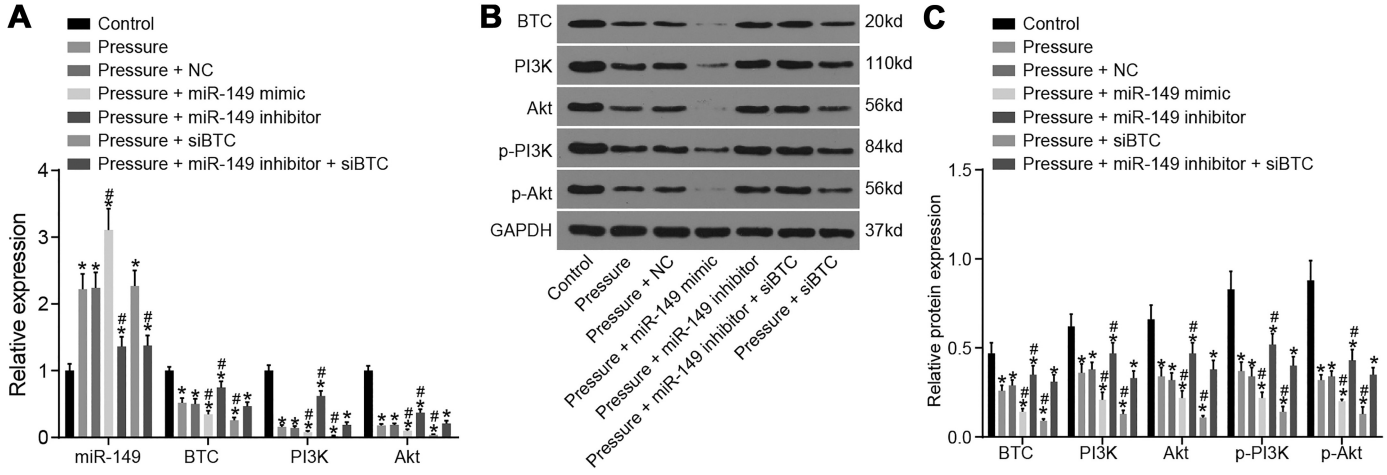

Fig. 7. RT-qPCR and Western blot analysis show that downregulation of miR-149 increases expression levels of BTC, PI3K, and Akt in RGCs. *A*: RT-qPCR was used to determine miR-149 expression and mRNA expression of BTC, PI3K, and Akt. *B*: protein bands of BTC, PI3K, p-PI3K, Akt, and p-Akt using Western blot analysis. *C*: protein levels of BTC, PI3K, p-PI3K, Akt, and p-Akt using Western blot analysis. $*P < 0.05$ vs. control group; $\#P < 0.05$ vs. pressure group and pressure + NC group. Measurement data are expressed as means ± SD; one-way analysis of variance was used to analyze data; the experiment was repeated 3 times. BTC, betacellulin; miR-149, microRNA-149; PI3K, phosphatidylinositol-3-kinase; NC, negative control; RGCs, retinal ganglion cells.

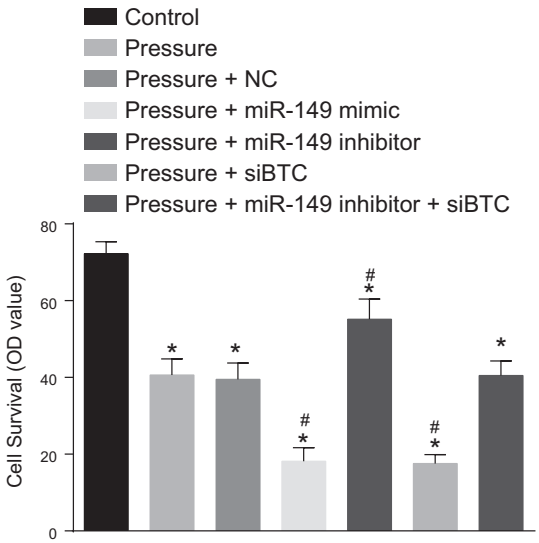

Fig. 8. CCK-8 assay shows that silencing miR-149 promotes RGC viability. *$P < 0.05$ vs. control group; #$P < 0.05$ vs. pressure group and the pressure + NC group. Measurement data are expressed as means ± SD; one-way analysis of variance was used to analyze data; the experiment was repeated 3 times. BTC, betacellulin; CCK-8, cell counting kit-8; miR-149, microRNA-149; NC, negative control; RGCs, retinal ganglion cells.

volvement in the prevention of the apoptosis of RGCs (26). The present study placed emphases on the effects of miR-149 on RGC proliferation and apoptosis in glaucoma through the PI3K/Akt signaling pathway.

Initially, our study detected that the EIOP mouse models displayed increased miR-149 expression and decreased BTC expression, as well as a reduced number of RGCs, when compared with the normal mice counterparts. Evidence has previously been presented demonstrating that a series of miRNAs are associated with the retina development, such as retinogenesis, retinal homeostasis, and retinal damage in human visual systems (10, 16). MiRNAs represent a class of critical regulators involved in the progression of glaucoma, which are also involved in biological processes of genes related to glaucoma (11). Romano et al. (28) employed in silico approaches to predict miRNA regulation in glaucoma and concluded that multiple miRNAs are potential biomarkers of which could be therapeutic targets in glaucoma. A previous study reported that several miRNAs display upregulated levels, including that of miR-4295, miR-92A-2–5P, and miR-4449, in glaucoma (35). In regard to miR-149, it has different expression patterns and cellular functions involved in the modulation of angiogenesis. Furthermore, genes under the control of miR-149 regulate cell differentiation, proliferation, migration, and adhesion, as well as morphogenesis (5). Izzotti et al. (14) revealed that miR-149 could maintain homeostasis between endothelia and extracellular matrix, however it is easily affected by damaged trabecular meshwork cells because of oxidative stress, ultimately leading to abnormal expression in retina. On the basis of bioinformatics prediction and dual luciferase reporter gene assay, BTC is directly targeted and negatively regulated by miR-149, with silencing of miR-149 resulting in ascended BTC expression. BTC belongs to an epidermal growth factor (EGF) family and plays a crucial role in regulating retinal vascular permeability as well as aiding in the facilitation of neural stem cell proliferation and the enhancement of neurogenesis (34, 38). Moreover, as a glycosylated (*N*- and *O*-linked) protein, BTC has proliferative effects on retinal pigment epithelial cells, which was indicated to be closely associated with the etiology and pathogenesis of retinal vascular leakage (2). Besides, Duex et al. (13) demonstrated a close correlation between miR-7 and the EGF receptor expression in tumorigenic activity of cancer cells. All the aforementioned literature was determined to be parallel to the results obtained during the present study in that BTC plays a significant role in the RGCs of retinal tissues of mouse with glaucoma as a target gene of miR-149.

Additionally, the data obtained indicated that the EIOP mouse models displayed reduced expression levels of PI3K

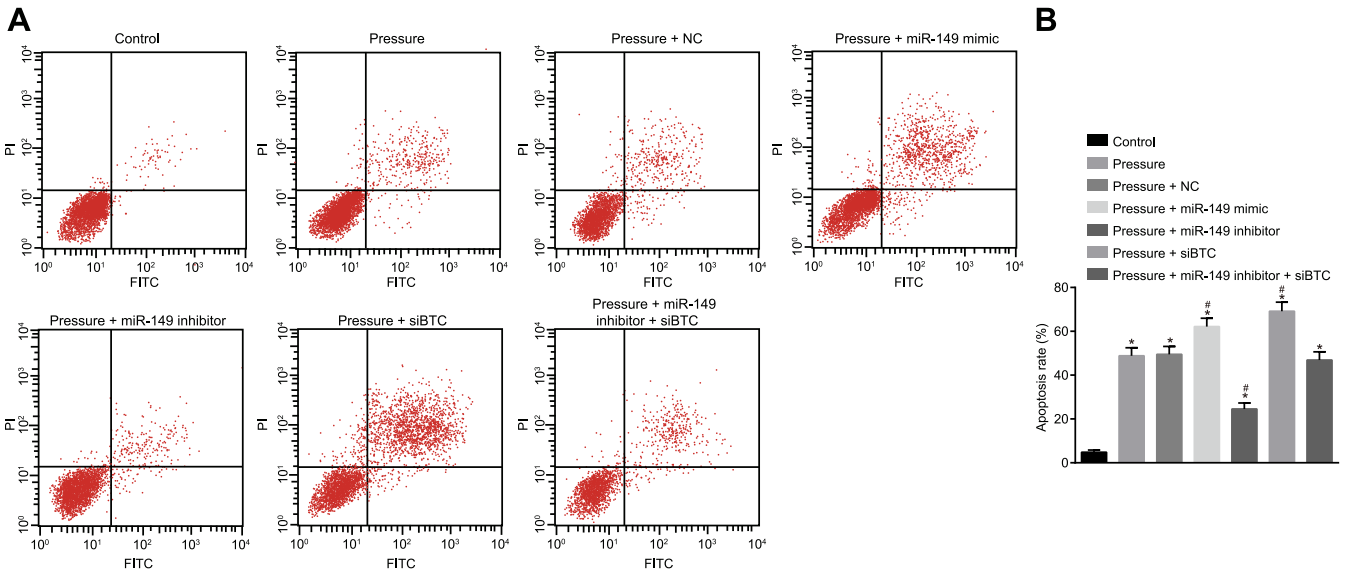

Fig. 9. Flow cytometry shows that downregulation of miR-149 inhibits RGC apoptosis. *A*: RGC apoptosis in each group. *B*: apoptotic rate of RGCs in each group. *$P < 0.05$ vs. control group; #$P < 0.05$ vs. pressure and pressure + NC groups. Measurement data are expressed as means ± SD; one-way analysis of variance was used to analyze data; the experiment was repeated 3 times. BTC, betacellulin; miR-149, microRNA-149; NC, negative control; RGCs, retinal ganglion cells.

and Akt and that downregulation of miR-149 increases the expression levels of PI3K and Akt, suggesting that silencing miR-149 promotes activation of the PI3K/Akt signaling pathway. Similarly, Li et al. (17) also previously asserted that PI3K/Akt expression levels are inhibited in mice with glaucoma. Previous reports have demonstrated a negative association between the expression of miR-218 and the PI3K/Akt/mammalian target of rapamycin (mTOR_ signaling pathway activity (41), suggesting that the inhibition of miR-218 could activate the PI3K/Akt/mTOR signaling pathway, which was again consistent with the findings of the present study. Furthermore, based on our findings we subsequently asserted that the downregulation of miR-149 promotes RGC viability and inhibits RGC apoptosis. Previous studies have indicated that miR-149, as a proapoptotic miR, promotes the process of apoptosis in human cancer cells (20), suggesting that downregulation of miR-149 could repress apoptosis. Moreover, Akt1, as a downstream target of miR-149 when repressed by miR-149 intensifies cell proliferation and the tumorigenicity of hepatocellular carcinoma (43), whereas the activation of the PI3K/Akt signaling pathway has been reported to effectively affect the role of BTC as a major c-erbB ligand involved in cell production and invasion (30). Ma et al. (22) have revealed that activation of the PI3K/Akt signaling pathway plays an inhibitory role in apoptosis. Furthermore, Qi et al. (26) demonstrated there to be a suppression of RGC apoptosis after ischemia-reperfusion because of the activation of the PI3K/Akt signaling pathway. All these findings support the position that downregulation of miR-149 promotes RGC viability and inhibits RGC apoptosis via activation of the PI3K/Akt signaling pathway.

Taken together, key observations were made suggesting that downregulation of miR-149 contributes to the suppression of RGC apoptosis by targeting BTC through the PI3K/Akt signaling pathway in glaucoma. These findings indicate that inhibition of miR-149 might be effective for the prevention of RGC apoptosis. Therefore, this study presents a promising new strategy for novel glaucoma therapy on a molecular level. However, certain limitations were faced during the present study, because of sample size and time constraints; as a result of this, further studies are required to elucidate fully the specific mechanisms of miR-149 in glaucoma through the PI3K/Akt signaling pathway.

DISCLOSURES

No conflicts of interest, financial or otherwise, are declared by the authors.

AUTHOR CONTRIBUTIONS

X.-G.N. and Y.-X.H. conceived and designed research; D.-S.F., Y.-X.H., and Y.-Y.H. performed experiments; B.-L.D. analyzed data; X.-G.N., D.-S.F., and F.G. interpreted results of experiments; Y.-X.H. prepared figures; Y.-Y.H. and F.G. drafted manuscript; X.-G.N., D.-S.F., and B.-L.D. edited and revised manuscript; X.-G.N., D.-S.F., Y.-X.H., Y.-Y.H., B.-L.D., and F.G. approved final version of manuscript.

REFERENCES

1. **Agapova OA, Malone PE, Hernandez MR.** A neuroactive steroid 5alpha-androstane-3alpha,17beta-diol regulates androgen receptor level in astrocytes. *J Neurochem* 98: 355–363, 2006. doi:10.1111/j.1471-4159.2006.03879.x.
2. **Anand-Apte B, Ebrahem Q, Cutler A, Farage E, Sugimoto M, Hollyfield J, Folkman J.** Betacellulin induces increased retinal vascular permeability in mice. *PLoS One* 5: e13444, 2010. doi:10.1371/journal.pone.0013444.
3. **Anshu A, Price MO, Richardson MR, Segu ZM, Lai X, Yoder MC, Price FW JR.** Alterations in the aqueous humor proteome in patients with a glaucoma shunt device. *Mol Vis* 17: 1891–1900, 2011.
4. **Baudouin C.** Detrimental effect of preservatives in eyedrops: implications for the treatment of glaucoma. *Acta Ophthalmol* 86: 716–726, 2008. doi:10.1111/j.1755-3768.2008.01250.x.
5. **Chamorro-Jorganes A, Araldi E, Rotllan N, Cirera-Salinas D, Suárez Y.** Autoregulation of glypican-1 by intronic microRNA-149 fine tunes the angiogenic response to FGF2 in human endothelial cells. *J Cell Sci* 127: 1169–1178, 2014. doi:10.1242/jcs.130518.
6. **Chen J, Qiu M, Dou C, Cao Z, Dong S.** MicroRNAs in bone balance and osteoporosis. *Drug Dev Res* 76: 235–245, 2015. doi:10.1002/ddr.21260.
7. **Chen Z, Song Y, Yao J, Weng C, Yin ZQ.** Alterations of sodium and potassium channels of RGCs in RCS rat with the development of retinal degeneration. *J Mol Neurosci* 51: 976–985, 2013. doi:10.1007/s12031-013-0082-9.
8. **Dahlhoff M, Algül H, Siveke JT, Lesina M, Wanke R, Wartmann T, Halangk W, Schmid RM, Wolf E, Schneider MR.** Betacellulin protects from pancreatitis by activating stress-activated protein kinase. *Gastroenterology* 138: 1585–1594.e3, 2010. doi:10.1053/j.gastro.2009.12.045.
9. **Engin KN, Yemişci B, Yiğit U, Ağaçhan A, Coşkun C.** Variability of serum oxidative stress biomarkers relative to biochemical data and clinical parameters of glaucoma patients. *Mol Vis* 16: 1260–1271, 2010.
10. **Genini S, Guziewicz KE, Beltran WA, Aguirre GD.** Altered miRNA expression in canine retinas during normal development and in models of retinal degeneration. *BMC Genomics* 15: 172, 2014. doi:10.1186/1471-2164-15-172.
11. **Guo R, Shen W, Su C, Jiang S, Wang J.** Relationship between the pathogenesis of glaucoma and miRNA. *Ophthalmic Res* 57: 194–199, 2017. doi:10.1159/000450957.
12. **Hertz J, Robinson R, Valenzuela DA, Lavik EB, Goldberg JL.** A tunable synthetic hydrogel system for culture of retinal ganglion cells and amacrine cells. *Acta Biomater* 9: 7622–7629, 2013. doi:10.1016/j.actbio.2013.04.048.
13. **Ingham PW, Nakano Y, Seger C.** Mechanisms and functions of Hedgehog signalling across the metazoa. *Nat Rev Genet* 12: 393–406, 2011. doi:10.1038/nrg2984.
14. **Izzotti A, Ceccaroli C, Longobardi MG, Micale RT, Pulliero A, La Maestra S, Saccà SC.** Molecular damage in glaucoma: from anterior to posterior eye segment. The microRNA role. *MicroRNA* 4: 3–17, 2015. doi:10.2174/2211536604666150707124640.
15. **Jiang LP, He CY, Zhu ZT.** Role of microRNA-21 in radiosensitivity in non-small cell lung cancer cells by targeting PDCD4 gene. *Oncotarget* 8: 23675–23689, 2017. doi:10.18632/oncotarget.15644.
16. **Kong N, Lu X, Li B.** Downregulation of microRNA-100 protects apoptosis and promotes neuronal growth in retinal ganglion cells. *BMC Mol Biol* 15: 25, 2014. doi:10.1186/s12867-014-0025-1.
17. **Li HB, You QS, Xu LX, Sun LX, Abdul Majid AS, Xia XB, Ji D.** Long non-coding RNA-MALAT1 mediates retinal ganglion cell apoptosis through the PI3K/Akt signaling pathway in rats with glaucoma. *Cell Physiol Biochem* 43: 2117–2132, 2017. doi:10.1159/000484231.
18. **Li SY, Yau SY, Chen BY, Tay DK, Lee VW, Pu ML, Chan HH, So KF.** Enhanced survival of melanopsin-expressing retinal ganglion cells after injury is associated with the PI3 K/Akt pathway. *Cell Mol Neurobiol* 28: 1095–1107, 2008. doi:10.1007/s10571-008-9286-x.
19. **Liao Q, Wang DH, Sun HJ.** Association of genetic polymorphisms of eNOS with glaucoma. *Mol Vis* 17: 153–158, 2011.
20. **Lin RJ, Lin YC, Yu AL.** miR-149* induces apoptosis by inhibiting Akt1 and E2F1 in human cancer cells. *Mol Carcinog* 49: 719–727, 2010. doi:10.1002/mc.20647.
21. **Liu Q, Ju WK, Crowston JG, Xie F, Perry G, Smith MA, Lindsey JD, Weinreb RN.** Oxidative stress is an early event in hydrostatic pressure induced retinal ganglion cell damage. *Invest Ophthalmol Vis Sci* 48: 4580–4589, 2007. doi:10.1167/iovs.07-0170.
22. **Ma Y, Qin H, Cui Y.** MiR-34a targets GAS1 to promote cell proliferation and inhibit apoptosis in papillary thyroid carcinoma via PI3K/Akt/Bad pathway. *Biochem Biophys Res Commun* 441: 958–963, 2013. doi:10.1016/j.bbrc.2013.11.010.
23. **Molasy M, Walczak A, Szaflik J, Szaflik JP, Majsterek I.** MicroRNAs in glaucoma and neurodegenerative diseases. *J Hum Genet* 62: 105–112, 2017. doi:10.1038/jhg.2016.91.

24. **Orlans FB.** Ethical decision making about animal experiments. *Ethics Behav* 7: 163–171, 1997. doi:10.1207/s15327019eb0702_7.
25. **Pan SJ, Zhan SK, Pei BG, Sun QF, Bian LG, Sun BM.** MicroRNA-149 inhibits proliferation and invasion of glioma cells via blockade of AKT1 signaling. *Int J Immunopathol Pharmacol* 25: 871–881, 2012. doi:10.1177/039463201202500405.
26. **Qi Y, Chen L, Zhang L, Liu WB, Chen XY, Yang XG.** Crocin prevents retinal ischaemia/reperfusion injury-induced apoptosis in retinal ganglion cells through the PI3K/AKT signalling pathway. *Exp Eye Res* 107: 44–51, 2013. doi:10.1016/j.exer.2012.11.011.
27. **Quigley HA.** Glaucoma. *Lancet* 377: 1367–1377, 2011. doi:10.1016/S0140-6736(10)61423-7.
28. **Romano GL, Platania CB, Forte S, Salomone S, Drago F, Bucolo C.** MicroRNA target prediction in glaucoma. *Prog Brain Res* 220: 217–240, 2015. doi:10.1016/bs.pbr.2015.04.013.
29. **Russo R, Adornetto A, Cavaliere F, Varano GP, Rusciano D, Morrone LA, Corasaniti MT, Bagetta G, Nucci C.** Intravitreal injection of forskolin, homotaurine, and L-carnosine affords neuroprotection to retinal ganglion cells following retinal ischemic injury. *Mol Vis* 21: 718–729, 2015.
30. **Shi L, Wang L, Wang B, Cretoiu SM, Wang Q, Wang X, Chen C.** Regulatory mechanisms of betacellulin in CXCL8 production from lung cancer cells. *J Transl Med* 12: 70, 2014. doi:10.1186/1479-5876-12-70.
31. **Solheim MH, Clermont AC, Winnay JN, Hallstensen E, Molven A, Njølstad PR, Rødahl E, Kahn CR.** Iris malformation and anterior segment dysgenesis in mice and humans with a mutation in PI 3-kinase. *Invest Ophthalmol Vis Sci* 58: 3100–3106, 2017. doi:10.1167/iovs.16-21347.
32. **SooHoo JR, Seibold LK, Laing AE, Kahook MY.** Bleb morphology and histology in a rabbit model of glaucoma filtration surgery using Ozurdex® or mitomycin-C. *Mol Vis* 18: 714–719, 2012.
33. **Sorkhabi R, Ghorbanihaghjo A, Javadzadeh A, Rashtchizadeh N, Moharrery M.** Oxidative DNA damage and total antioxidant status in glaucoma patients. *Mol Vis* 17: 41–46, 2011.
34. **Sugimoto M, Cutler A, Shen B, Moss SE, Iyengar SK, Klein R, Folkman J, Anand-Apte B.** Inhibition of EGF signaling protects the diabetic retina from insulin-induced vascular leakage. *Am J Pathol* 183: 987–995, 2013. doi:10.1016/j.ajpath.2013.05.017.
35. **Tanaka Y, Tsuda S, Kunikata H, Sato J, Kokubun T, Yasuda M, Nishiguchi KM, Inada T, Nakazawa T.** Profiles of extracellular miRNAs in the aqueous humor of glaucoma patients assessed with a microarray system. *Sci Rep* 4: 5089, 2014. doi:10.1038/srep05089.
36. **Wang Y, Zheng X, Zhang Z, Zhou J, Zhao G, Yang J, Xia L, Wang R, Cai X, Hu H, Zhu C, Nie Y, Wu K, Zhang D, Fan D.** MicroRNA-149 inhibits proliferation and cell cycle progression through the targeting of ZBTB2 in human gastric cancer. *PLoS One* 7: e41693, 2012. doi:10.1371/journal.pone.0041693.
37. **Winzeler A, Wang JT.** Purification and culture of retinal ganglion cells from rodents. *Cold Spring Harb Protoc* 2013: 643–652, 2013. doi:10.1101/pdb.prot074906.
38. **Xia J, Luo M, Ni N, Chen J, Hu Y, Deng Y, Ji J, Zhou J, Fan X, Gu P.** Bone marrow mesenchymal stem cells stimulate proliferation and neuronal differentiation of retinal progenitor cells. *PLoS One* 8: e76157, 2013. doi:10.1371/journal.pone.0076157.
39. **Xu Y, Chen X, Lin L, Chen H, Yu S, Li D.** MicroRNA-149 is associated with clinical outcome in human neuroblastoma and modulates cancer cell proliferation through Rap1 independent of MYCN amplification. *Biochimie* 139: 1–8, 2017. doi:10.1016/j.biochi.2017.04.011.
40. **Yang Y, Choi PP, Smith WW, Xu W, Ma D, Cordner ZA, Liang NC, Moran TH.** Exendin-4 reduces food intake via the PI3K/AKT signaling pathway in the hypothalamus. *Sci Rep* 7: 6936, 2017. doi:10.1038/s41598-017-06951-0.
41. **Zhang X, Shi H, Tang H, Fang Z, Wang J, Cui S.** miR-218 inhibits the invasion and migration of colon cancer cells by targeting the PI3K/Akt/mTOR signaling pathway. *Int J Mol Med* 35: 1301–1308, 2015. doi:10.3892/ijmm.2015.2126.
42. **Zhang XM, Li Liu DT, Chiang SW, Choy KW, Pang CP, Lam DS, Yam GH.** Immunopanning purification and long-term culture of human retinal ganglion cells. *Mol Vis* 16: 2867–2872, 2010.
43. **Zhang Y, Guo X, Xiong L, Yu L, Li Z, Guo Q, Li Z, Li B, Lin N.** Comprehensive analysis of microRNA-regulated protein interaction network reveals the tumor suppressive role of microRNA-149 in human hepatocellular carcinoma via targeting AKT-mTOR pathway. *Mol Cancer* 13: 253, 2014. doi:10.1186/1476-4598-13-253.
44. **Zhong X, Coukos G, Zhang L.** miRNAs in human cancer. *Methods Mol Biol* 822: 295–306, 2012. doi:10.1007/978-1-61779-427-8_21.
45. **Zhou L, Xie Y, Li S, Liang Y, Qiu Q, Lin H, Zhang Q.** Rapamycin prevents cyclophosphamide-induced over-activation of primordial follicle pool through PI3K/Akt/mTOR signaling pathway in vivo. *J Ovarian Res* 10: 56, 2017. doi:10.1186/s13048-017-0350-3.
46. **Zhou Y, Li S, Li J, Wang D, Li Q.** Effect of microRNA-135a on cell proliferation, migration, invasion, apoptosis and tumor angiogenesis through the IGF-1/PI3K/Akt signaling pathway in non-small cell lung cancer. *Cell Physiol Biochem* 42: 1431–1446, 2017. doi:10.1159/000479207.